Fuel 428 (2027) 140264

Contents lists available at ScienceDirect

Fuel

journal homepage: www.elsevier.com/locate/fuel

Full Length Article

Synergistic enhancement of heat transfer and formation kinetics of hydrogen hydrates by stainless steel fibers and SDS

Siyuan Chen [a], Yanhong Wang [a,b,*], Shuanshi Fan [a,b], Xuemei Lang [a,c], Gang Li [a]

[a] School of Chemistry and Chemical Engineering, South China University of Technology, Guangzhou 510640, China
[b] Key Laboratory of Heat and Mass Transfer and Low-Carbon Conversion, Ministry of Education, South China University of Technology, Guangzhou 510640, China
[c] Key Laboratory of Fuel Cell Technology of Guangdong Province, Guangzhou 510640, China

ARTICLE INFO

Keywords:
Gas hydrate
Hydrogen storage
Stainless steel fiber
Heat transfer
Quasi-simultaneous formation

ABSTRACT

Rapid formation kinetics is critical for advancing hydrate-based hydrogen storage technology. However, accelerated hydrate growth inevitably intensifies hydration heat accumulation, which imposes strong thermal inhibition on subsequent hydrogen hydrate growth. Based on the quasi-simultaneous formation of propane–hydrogen hydrates, this work introduced stainless steel fibers (SSF) to address the heat transfer bottleneck, and explored the synergistic promotion with sodium dodecyl sulfate (SDS). The synergistic effect between SSF and SDS was highly dependent on SDS concentration, and the optimal performance was achieved at 0.03 wt% SDS. Compared with other SDS concentrations, the hydrogen uptake was increased by 9.09 %–11.94 %, and the average hydrate growth rate was enhanced by 25.30 %–57.65 %. The optimal SSF dosage was determined to be 5.0 wt%, which sufficiently covers the gas–liquid interface and supports continuous hydrate growth. Moreover, longer SSF with a more continuous linear thermal conduction network exhibited superior heat dissipation behavior than shorter fibers. Under the optimal conditions, the maximum hydrogen uptake reached 69.80 cm^3/cm^3 hydrate within only 13 min, and the average hydrate growth rate was up to 483.23 $\times$ 10^{-2} cm^3/cm^3 hydrate·min^{-1}, representing the fastest hydrogen hydrate formation kinetics reported so far. Heat transfer analysis demonstrated that the macroscopic effective thermal conductivity changed little, but the dominant internal thermal resistance was nearly eliminated, and the heat removal rate was improved by approximately 18.1 times, favoring sustained hydrogen hydrate growth. This study provides a feasible and efficient strategy for kinetic and thermal enhancement of hydrate-based hydrogen storage systems.

1. Introduction

Hydrogen, as a clean and efficient energy carrier, demonstrates outstanding performance in environmental issues, which is regarded as one of the promising energy carriers to replace fossil fuels. Hydrogen storage technology plays a crucial role in the hydrogen industry chain. Compared with traditional technologies such as liquefied hydrogen and compressed hydrogen, hydrate-based hydrogen storage technology exhibits favorable prospects as the advantages of high storage capacity potential, reversible storage/release process, and low costs [1].

However, the issue of harsh formation conditions greatly reduce the application potential. Mao et al. [2] demonstrated that hydrogen hydrates can only be stable under extreme conditions of 200–300 MPa, which meant that the commercial application of pure hydrogen hydrates is unfeasible. Florusse et al. [3] provided a new insight for its commercial application. They reported that tetrahydrofuran (THF) could co-occupy the hydrate cages with hydrogen, reducing the pressure from 300 MPa to 5 MPa at 279.6 K. Such compounds that could significantly lower the formation conditions are called thermodynamic promoters. Extensive research focused on the hydrogen-thermodynamic promoter hydrates [4–8]. And gases such as methane [9,10], propane [11–13], and sulfur hexafluoride [14,15] have been proven that also acted as thermodynamic promoters to promote hydrogen hydrates formation under mild conditions. Among the common thermodynamic promoters, THF can significantly reduce the formation pressure but is volatile, toxic, and easily soluble in water, leading to poor recyclability and potential environmental risks. Cyclopentane (CP) shows low toxicity but immiscible with water and forms a separate oil phase, which limits mass transfer and unsuitable for static reaction systems. In contrast, propane is a non-toxic, low-cost gaseous promoter that can co-

* Corresponding author at: School of Chemistry and Chemical Engineering, South China University of Technology, Guangzhou 510640, China.
E-mail address: wyh@scut.edu.cn (Y. Wang).

https://doi.org/10.1016/j.fuel.2026.140264
Received 22 April 2026; Received in revised form 12 May 2026; Accepted 4 June 2026
Available online 12 June 2026

occupy hydrate cages with hydrogen under moderate conditions, shows good compatibility with gas–liquid interfaces in static systems. Therefore, propane was considered as a suitable thermodynamic promoter to achieve stable formation of hydrogen hydrates with high efficiency and safety.

Notably, although thermodynamic promoters satisfy the mild thermodynamic conditions for hydrogen hydrates, the kinetic issues of low storage capacity and slow storage rate are the primary obstacles for further development [16]. Therefore, an effective method is needed to enhance hydrogen hydrates formation. Currently, metals or metal oxide nanoparticles [17–22] have been proven to effectively promote hydrate nucleation and growth as the characteristics of abundant nucleation sites and excellent thermal conductivity of these materials. However, the heat transfer mode of such materials is distributed point-strengthening, resulting in discontinuous heat transfer process that affect subsequent hydrate growth. Deng et al. [23] found that a small amount of (only 7.6 % compared with other metal materials) stainless steel fibers (SSF) could increase the gas storage capacity by 145.4 %. Yang et al. [24] also demonstrated that SSF with linear structures and excellent thermal conductivity could enable continuous linear heat transfer enhancement, shortening the formation time and improving storage capacity/rate, which indicated the promoting effect of SSF on hydrate nucleation and growth.

Critically, SSF was just applied in CH_4 or CO_2 hydrates, not the field of hydrogen hydrates, mainly because the unique nucleation mode of hydrogen hydrates: progressive nucleation [25], which hydrogen hydrate crystallites are continuously nucleated during the growth process. And the hydrate growth rate is limited by the hydrogen hydrate nucleation rate [26]. So the heat transfer of hydrogen hydrates is often ignored as the characteristics of slow hydrate growth with almost no hydration heat accumulation. In our prior research [25], we proposed a novel method called quasi-simultaneous formation (q-SF) to alter the inherent nucleation mode of hydrogen hydrates, breaking the limitation of the crystal nuclei quantity during the hydrate growth process, with the rapid hydrogen hydrate growth process. However, the rapid growth process of hydrogen hydrates lead to prominent hydration heat issues, resulting in thermal inhibition for further growth of hydrogen hydrates. And the inhibition effect of hydration heat would be sharper with the faster initial hydrate growth. So with the method of q-SF to promote hydrogen hydrates formation, the issue of hydration heat cannot be ignored. But whether the thermally conductive material SSF could enhance heat transfer to promote hydrogen hydrate q-SF kinetics remains unknown.

Therefore, based on the q-SF of hydrogen hydrates, we coupled SDS with SSF to promote the formation kinetics. At 18.2 MPa and 274.15 K, we investigated the effect of SDS concentrations and SSF parameters on hydrogen hydrate formation to identify the optimal operating conditions. And the mechanism of SSF on the hydrogen hydrate formation was further indicated to show the technical feasibility of SSF-SDS coupling in promoting hydrogen hydrate formation kinetics, which provides the insight for advancing hydrogen storage technology.

2. Experimental

2.1. Materials

316 L stainless steel fiber was fabricated via a series of complex processes including surface treatment, bundling, drawing, heat treatment and electrolytic separation. It maintains the inherent metallic properties, and exhibits excellent thermal conductivity (52 $W{\cdot}m^{-1}{\cdot}K^{-1}$), as well as favorable flexibility and high specific surface area similar to textile fibers. The stainless steel fibers with specifications of φ 6.5 μm × 3 mm and φ 6.5 μm × 100 mm were provided by Hunan Huitong Advance Materials Co., Ltd; Sodium dodecyl sulfate (purity of 99.0 %) was purchased from Aladdin Biochemical Technology (Shanghai) Co., Ltd; Deionized water obtained in the laboratory was used for all the experiments.

2.2. Apparatus and procedures

Fig. 1 shows the schematic diagram of the experimental apparatus in this study. The experimental setup used for hydrogen hydrate formation was similar to the one described in our previous research [25]. The effective volume of the main reactor is 100 mL, and this study adopt a static reaction system without any stirring during the entire experimental process.

The solution (deionized water or SDS solution) was firstly added to the reaction vessel, followed by a certain mass fraction of SSF to ensure full contact with both the liquid and gas phases. The total mass of the system was controlled at approximately 10 g. The temperature was set to the experimental temperature (274.15 K). And propane (0.45 MPa) and hydrogen were injected successively (total pressure of 18.2 MPa), adjusting the gas distribution at the interface to ensure the q-SF of hydrogen hydrates. The system was depressurized and decomposed after hydrate formation for analyzing the gas composition in the hydrate phase. Detailed experimental and calculation procedures can be referred to our previous research [25].

2.3. Calculation of effective thermal conductivity

A model based on the following assumptions was proposed to calculate the effective thermal conductivity (ETC) of hydrogen hydrate filled with SSF:

(1) The contact thermal resistance between hydrate crystals and reactor walls are negligible.
(2) The micro-interactions between hydrate crystals and SSF are negligible.
(3) Hydrate crystals and SSF exhibit uniform spatial distribution, with no convective or radiative heat transfer.

The thermal conductivity of the hydrate-SSF system can be expressed as [27]:

$$\lambda_e = \lambda_e^{H/S} \tag{1}$$

In Eq. (1), the superscripts H and S denote hydrate and stainless steel fiber, respectively.$\lambda_e^{H/S}$ represents the thermal conductivity of the Hydrate-SSF system, $W{\cdot}m^{-1}{\cdot}K^{-1}$, which can be expressed by the Maxwell model [28] as:

$$\lambda_e^{H/S} = \lambda_H \cdot \frac{\lambda_S + 2\lambda_H - 2\varphi(\lambda_H - \lambda_S)}{\lambda_S + 2\lambda_H + \varphi(\lambda_H - \lambda_S)} \tag{2}$$

where λ_H is the thermal conductivity of propane-hydrogen hydrate, λ_S is the thermal conductivity of SSF, and φ is the SSF volume fraction of the system.

In this study, the thermal conductivity of propane-hydrogen hydrates at the experimental temperature of 274.15 K was taken as 0.57 $W{\cdot}m^{-1}{\cdot}K^{-1}$ as the loose and porous structures [29]. The thermal conductivity of SSF was taken as 52 $W{\cdot}m^{-1}{\cdot}K^{-1}$. And φ was primarily expressed by Eq. (3):

$$\varphi = \frac{V_S}{V_H + V_S} \tag{3}$$

where V_S and V_H represent the volume of SSF and hydrate (L), respectively, which can be calculated by Eq. (4) and (5):

$$V_S = \pi r_1^2 \cdot L_S \tag{4}$$

$$V_H = \frac{m_H}{\rho_H} = \frac{0.01}{920} = 1.087 \times 10^{-5} m^3. \tag{5}$$

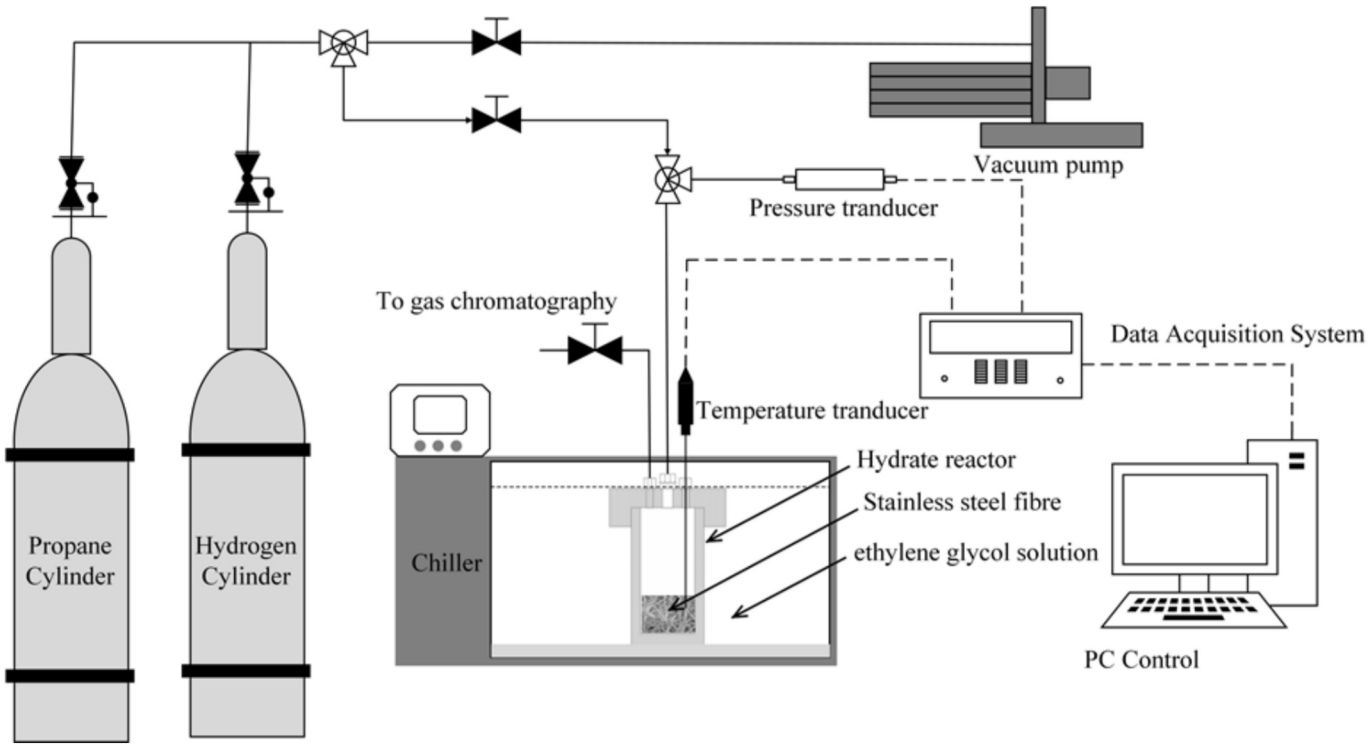

Fig. 1. Schematic diagram of the experimental apparatus.

where r_1 is the radius of SSF (3.25 μm). The linear density of SSF is given as 26.7 g/km. So the total Length of SSF (L_S) could be calculated by $L_S = \frac{m_S}{\rho_L} = \frac{0.5}{26.7\times10^{-6}} = 18.73m$

3. Results and discussion

3.1. Synergistic effect of SSF with SDS on the kinetics of hydrogen hydrates

Lower temperatures and higher pressures were favorable for the further formation of hydrogen hydrates. However, the heat accumulation of the rapid propane-hydrogen hydrate formation hinders the continuous growth of hydrates. SSF has been demonstrated to promote the hydrate formation as an effective thermal conductivity additive [23,24]. The structure of SSF was shown in Fig. 2a and SEM showed the microstructure and surface morphology of SSF (as shown in Fig. 2(b) and (c)). It could be shown that SSF with ample contact surface area formed an interconnected network structure for the diffusion of liquid water and heat transfer, and the interstices of SSF network can be regarded as the channels for gas diffusion. Also, SSF had a relatively rough surface, which would provide abundant nucleation sites for the hydrate nucleation. Therefore, the hydration system with SSF would be expected to high hydrogen storage rate and capacity.

Consequently, 1 g SSF was added to the hydrate system to accelerate heat transfer. Fig. 3a shows the temperature and pressure variations over time of the systems of pure water, pure water + SSF, SDS and SDS + SSF. Throughout the experiment, the pure water system exhibited the longest nucleation induction period with 568 min. The addition of either SDS or SSF drastically shortened the induction time to 176 min and 295 min, respectively. SDS promoted the hydrogen hydrate nucleation by reducing gas–liquid surface tension [30], while SSF showed similar promoting effect as the sufficient nucleation sites provided by its rough metal surface [23]. Furthermore, SDS and SSF exhibited a synergistic promoting effect, with the SDS + SSF system achieving an induction time of only 16 min. And the synergy arose from the distinct mechanisms of SDS and SSF—combined effects of reduced surface tension and increased nucleation sites significantly enhance the hydrate nucleation. It can also be observed that the corresponding temperature rise peaks of with SSF were smaller. Notably, although the water + SSF system presented a relatively high temperature rise peak, this phenomenon was accompanied by a continue hydrogen hydrates growing process upward

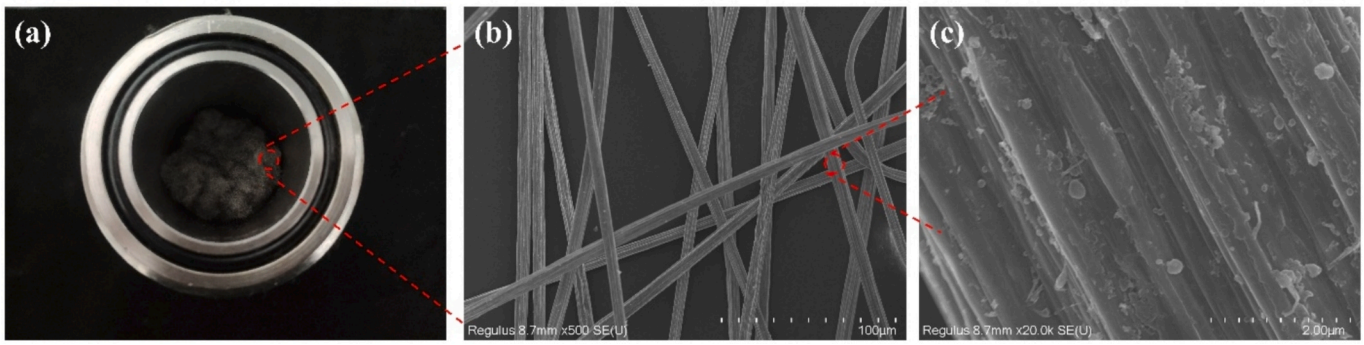

Fig. 2. (a) Stainless steel fiber sample, (b) SEM image (100 μm scale bar) and (c) SEM image (2 μm scale bar).

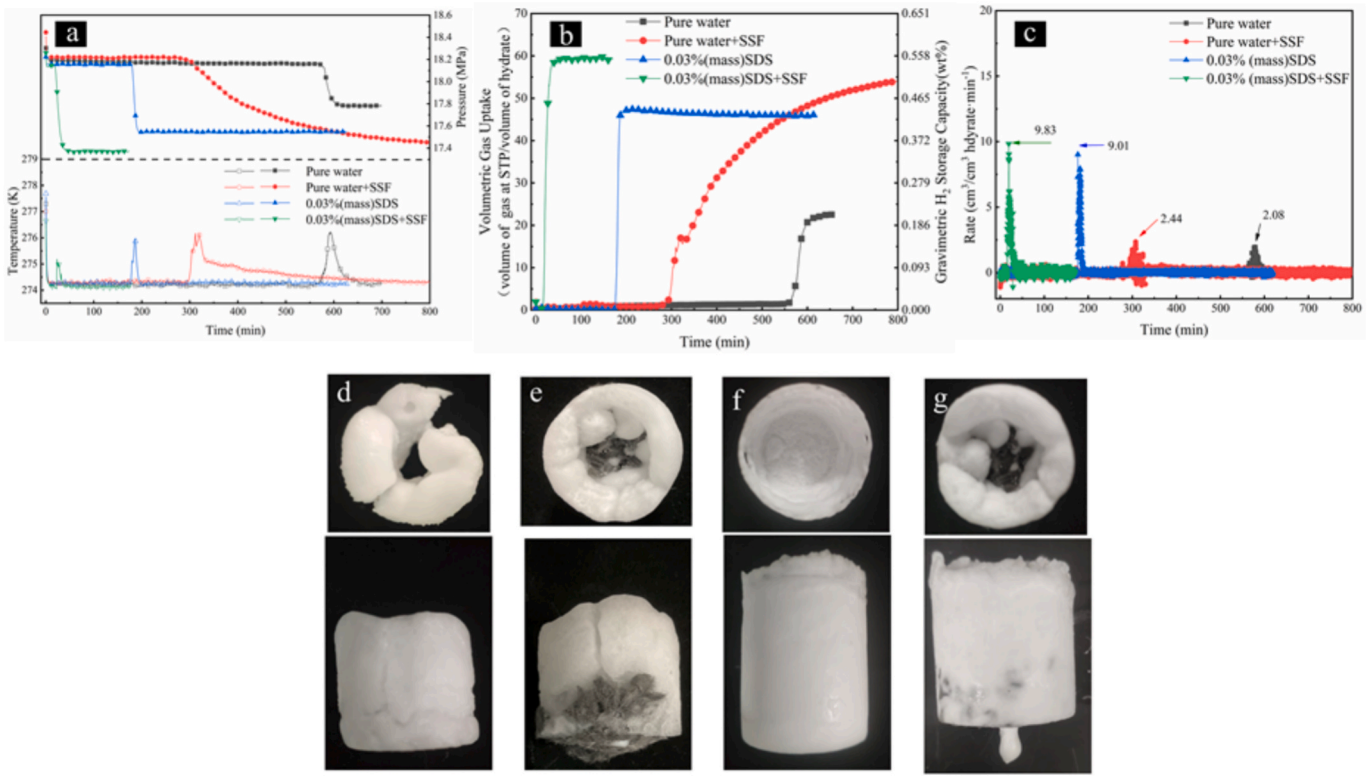

Fig. 3. (a) Variation of temperature and pressure, (b) hydrogen storage capacity, and (c) hydrogen storage rates during hydrate formation. (d − g) Morphologies of hydrogen-propane hydrate with or without SSF at 18.2 MPa and 274.15 K: (d) pure water without SSF, (e) pure water with SSF, (f) 0.03 %(mass) SDS without SSF, and (g) 0.03 %(mass) SDS with SSF.

along the SSF. And the SDS + SSF system exhibited a more obvious temperature drop (from 1.6 K to 0.9 K), which presents an extremely high hydrate growth rate and a drastically shortened formation period. Under such a rapid growth condition, SSF still effectively accelerates hydration heat dissipation through the interconnected thermally conductive network [31], mitigating temperature rise and avoiding stronger thermal inhibition that would occur without SSF. Therefore, the role of SSF in enhancing heat transfer remains significant and indispensable, even under fast kinetic conditions promoted by SDS.

Fig. 3b depicts the hydrogen storage capacity during q-SF of hydrogen hydrate across different systems. Under similar conditions, the pure water system exhibited the lowest hydrogen storage capacity (merely 22.5 cm^3/cm^3 hydrate, equivalent to 0.209 wt%), indicating incomplete conversion of water-to-hydrates. Under static conditions, the hydrate layer at the gas–liquid interface impeded the hydrogen diffusion into the inner liquid phase, preventing continuous hydrate growth. SDS would reduce the gas–liquid surface tension, resulting in a loose and porous hydrate structure that enhances mass transfer and enables continuous hydrogen hydrate growth [32]. While the incorporation of SSF altered the hydrogen hydrates growth behavior: compared to ~70 min growth period in the pure water system, the SSF system maintained a sustained growth process for nearly 500 min, achieving the storage capacity of 53.7 cm^3/cm^3 hydrate (0.500 wt%)—even higher than 46.01 cm^3/cm^3 hydrate (0.428 wt%) observed in the SDS system. When SDS was combined with SSF, the hydrate growth lasted only ~30 min, with a storage capacity reaching 59.75 cm^3/cm^3 hydrate (0.556 wt%), demonstrating that SDS and SSF also synergistically promoted the hydrate growth process.

Fig. 3c illustrates the instantaneous hydrogen storage rate during the q-SF of hydrogen hydrate in different systems. The storage rates for the pure water and pure water + SSF systems ranged from 2.1 to 2.5 cm^3/cm^3 hydrate·min^{-1}. While the addition of SDS increased the storage rates of both systems to above 9.0 cm^3/cm^3 hydrate·min^{-1}, highlighting the significant role of SDS in the rapid hydrate growth stage. In contrast, SSF had a weaker impact on both pure water and SDS systems, increasing the maximum rates by only 17.31 % and 9.1 %, respectively. This indicated that although SSF promoted hydrate growth to some extent by facilitating heat dissipation, it cannot trigger the rapid kinetic behavior in the initial stage (defined as the period of rapid nucleation and steep gas uptake rate rise). Combining the insights from Fig. 3 (b) and (c), it was reasonable to infer that SDS reduced the gas–liquid interfacial tension, enhanced mass transfer and altered the hydrate morphology (rendering it more porous) to enable rapid hydrate growth. In contrast, SSF primarily affected the continuous hydrate growth stage (defined as the period of steady long-term hydrate growth toward the bulk liquid): the interwoven SSF network provided a large surface area and supporting structure for liquid water diffusion, overcoming the limitations imposed by the hydrate layer in static systems. Hydrogen hydrates can continue growing upward along the SSF, leading to a higher conversion of water-to-hydrates—explaining the higher storage capacity in the pure water + SSF system. However, the slow diffusion rate of pure water on the SSF surface resulted in a relatively long growth period. SDS could enable rapid hydrate growth along both the reactor wall and SSF.

To further clarify the synergistic promoting effect of SSF and SDS on the hydrogen hydrate formation, the morphologies of hydrates formed at the end of the process are presented in Fig. 3 d–g. The pure water system exhibited a low conversion rate, limited by the surface hydrate layer that hindered further hydrate growth. In contrast, SDS induced a distinct growth pattern, with hydrates forming a porous structure along the reactor walls. Driven by capillary action [33,34], the SDS solution migrated from the bulk phase toward the gas phase through this porous hydrate structure, resulting in a hydrate sample consisting of only a bottom layer and a thin circular hydrate layer (Fig. 3f). The addition of SSF thickened the hydrate layer near the reactor wall, forming an SSF-supported hydrate framework. A portion of the hydrate grew near the

inner reactor wall (due to the preference for hydrate formation on metal surfaces), where hydration heat can be efficiently dissipated. Another portion hydrogen hydrates was formed as the SDS solution migrated upward through SSF to the top of the framework. In the SDS + SSF system, SDS promotes hydrate nucleation and rapid growth by reducing surface tension and modifying hydrate morphology, while SSF further enhances nucleation and growth through its abundant surface nucleation sites and interconnected network structure. Together, SSF and SDS exert a synergistic promoting effect on the hydrogen hydrate formation.

3.2. Influence of SDS concentration on the synergistic effect

Although extensive literature supports SDS as a kinetic promoter for hydrate formation, the existing qualitative understanding is system-specific. For unique guest substances, hydrate formation rates and final storage capacity are related to SDS concentration [35,36]. However, the universality of this dependence remains unclear, and the optimal surfactant concentration appears to be a characteristic parameter of the specific system under investigation. Therefore, this study experimentally determined the optimal SDS concentration (ranging from 0.01 % to 0.1 % by mass) for promoting the kinetics of hydrogen hydrate formation in the presence of SSF.

Fig. 4 compares the hydrogen storage capacity and storage rate variations for different SDS concentrations with and without SSF. Compared to the pure SDS systems, the addition of SSF significantly shortened the induction time (mostly to ~10 min), indicating that SSF promoted hydrate nucleation by providing a rough metal surface at the gas–liquid interface. As SDS concentration increased, the promoting effect of SSF on hydrate growth gradually diminished and eventually shifted to inhibition. Within the SDS concentration range of 0.01 %–0.03 % (mass), a promoting effect was observed: with hydrogen storage capacity increased by 62.82 % and 30.41 %, respectively. In contrast, within the range of 0.05 %–0.1 % (mass), an inhibition effect was noted: with hydrogen storage capacity decreased by 11.55 % and 17.42 %, respectively. Notably, when the SDS concentration reached 0.1 % (mass), the addition of SSF even reduced the hydrogen storage rate. These results demonstrated that the synergistic effect of SSF and SDS was highly dependent on SDS concentrations. Previous research by Chen et al. [25] suggested that in high-concentration SDS systems, the adsorption of SDS onto the hydrate layer via capillary action further enhanced the conversion of water into the hydrates, achieving higher hydrogen storage capacity. However, SSF may alter the process by influencing the arrangement of SDS at the interface [30]. The SDS solution grew upward along both the metal reactor wall and the SSF simultaneously. The main effect of SDS was reducing the interfacial tension. At 0.03 % (mass), SDS molecules were sufficiently adsorbed at the gas–liquid interface to achieve the lowest interfacial tension [37], which greatly promoted gas dissolution and hydrate nucleation [38]. Further increasing SDS concentration did not lower surface tension but instead caused partial aggregation [39], which increased the viscosity and interfacial resistance to hinder gas diffusion into the liquid phase [40]. Also at 0.03 wt%, SDS remained primarily at the interface rather than forming micelles in bulk solution, the capillary effect and water transport along SSF are maximized without excessive micelle entrapment, forming the most efficient heat–mass transfer pathways [41].

The hydrogen storage capacity, time required to reach 90 % of the

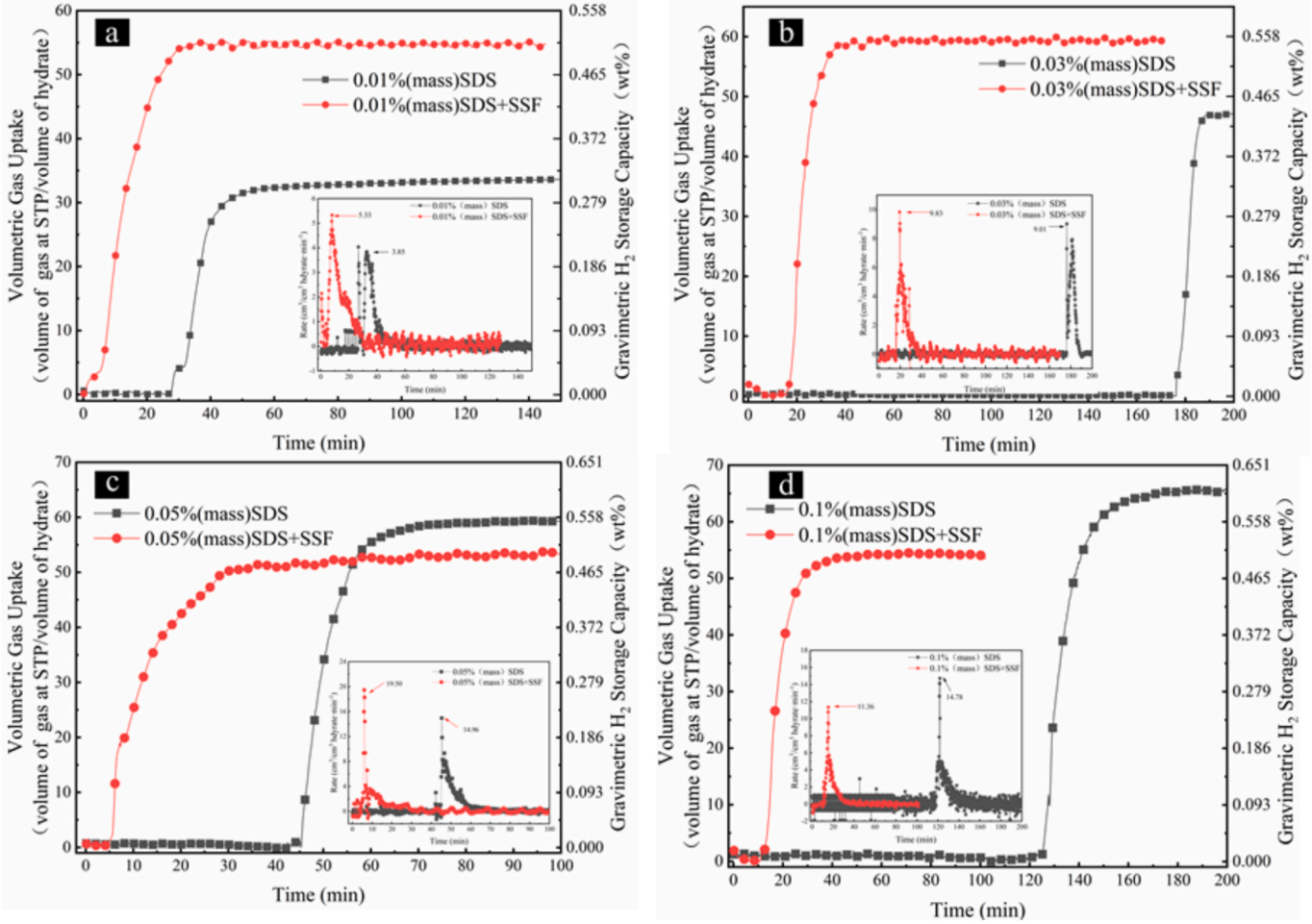

Fig. 4. The hydrogen storage capacity and storage rates of hydrogen hydrates with SSF in different SDS concentration solution (P = 18.2 MPa, T = 274.15 K).

maximum capacity (t_{90}), and average hydrate growth rate with different SDS concentrations in the SSF systems are shown in Fig. 5. When the SDS concentration reached 0.03 % (mass), the storage capacity achieved the maximum value of 60.0 cm^3/cm^3 hydrate (0.558 wt%), and a small hydrogen hydrates growth was realized with t_{90} only 14 min, and the average hydrate growth rate reached 384.11 × 10^{-2} cm^3/cm^3 hydrate·min^{-1}. Compared with the systems with other SDS concentrations, the hydrogen storage capacity increased by 9.09 %–11.94 %, and the growth rate increased even more significantly by 25.30 %–57.65 %. Considering the hydrogen storage performance comprehensively, 0.03 % (mass) SDS is regarded as the optimal concentration for promoting the formation of hydrogen hydrates with SSF.

3.3. Effect of SSF parameters on the kinetics of hydrogen hydrates

The promoting effect of SSF on hydrogen hydrate is associated with the mass transfer performance at the gas–liquid interface. Therefore, to fully exploit the potential of SSF, it is necessary to consider its coverage at the gas–liquid interface. Fig. 6 shows the temperature and pressure changes during hydrate formation for different SSF systems. As SSF increased from 2.5 % to 15 % (mass), the temperature rise peak decreased from 2.5 K to 0.45 K. This was primarily due to the high thermal conductivity of SSF, which enabled efficient dissipation of hydration heat and facilitated the further/continuous formation of hydrogen hydrates.

Fig. 7(a) and (b) depict the variations in hydrogen storage capacity and storage rate during hydrate formation for systems with different SSF loadings. For all SSF loadings systems investigated, the SSF was partially immersed in the aqueous phase and partially exposed to the gas phase in the reactor. 2.5 % (mass) SSF was sparsely distributed and could not fully cover the gas–liquid interface, with most fibers sinking at the bottom or adhering locally to the reactor wall, which prevented effective heat exchange. This system exhibited the highest temperature spike, and hydrogen hydrates could not grow upward along the SSF with some water unconverted, also resulting in the lowest storage capacity (only 46.25 cm^3/cm^3 hydrate, equivalent to 0.432 wt%). 5 % (mass) SSF formed a uniform interwoven network that fully covered the gas–liquid interface, with one end in the liquid phase and the other exposed to the gas phase, which favored water migration, gas diffusion, and heat dissipation simultaneously. This system achieved the highest hydrogen storage capacity of 68.09 cm^3/cm^3 hydrate (0.630 wt%). However, higher SSF loadings (10 % and 15 %) did not further enhance the hydrogen storage performance. This phenomenon primarily arose because the continuous migration of free water through the porous hydrate structure was easier than along the SSF [42]. Fig. 3 d–g also illustrated that hydrogen hydrates predominantly grew upward along the reactor wall, with only partial growth along the SSF. Additionally, since the top of the SSF was dry, free water must firstly be wicked by capillary forces before further hydrate formation can occur. Excessive SSF accumulated and overlapped severely. A large portion of fibers was fully immersed in water without exposure to the gas phase, which hindered capillary water migration and gas diffusion, thus weakening the promotion effect on hydrate growth.

Table 1 summarizes the hydrogen storage capacity, induction time, t_{90}, and average hydrate growth rate for systems with different SSF loadings. It could be shown that SSF significantly promoted the hydrate nucleation process, with induction times consistently ranging from 10 to 20 min. However, the induction time showed a slight upward trend with increasing SSF dosage. This phenomenon can be reasonably attributed to aggregation, insufficient interface exposure, and imperfect heat transfer network rather than a loss of thermal conductivity itself. Excessive SSF tend to aggregate and overlap, which reduced the effective specific surface area available for hydrate nucleation. And overdosed SSF cannot be fully dispersed and mostly remained fully immersed in the liquid phase rather than spanning the gas–liquid interface, weakening interfacial nucleation. And the promotional effect was optimized when SSF was sufficient to cover the gas–liquid interface (5 %), achieving dual promotion of hydrate nucleation and hydrate growth. Further increasing the loading did not improve the promotional effect. Notably, the 5 % (mass) SSF yielded the best hydrogen storage performance, with a maximum storage capacity of 68.09 cm^3/cm^3 hydrate (0.630 wt%) and an average hydrate growth rate of 235.70 × 10^{-2} cm^3/cm^3 hydrate·min^{-1}.

To compare the effects of SSF length on hydrate gas storage performance, long SSF (φ 6.5 μm × 100 mm) were used to test the promoting effect on hydrogen hydrates with 5 % (mass) loading. Fig. 8 presents the variations in temperature and pressure during the experiments, while Fig. 9 shows the hydrogen storage capacity and storage rate, respectively. The induction times for both systems were ~15 min, indicating similar capabilities to promote hydrate nucleation. And the both systems also showed similar temperature rise peak in Fig. 8. However, the storage rate profile (Fig. 9b) revealed that the maximum rate in the long SSF system (14.20 cm^3/cm^3 hydrate·min^{-1}) was significantly higher than that in the short SSF system (5.24 cm^3/cm^3 hydrate·min^{-1}),

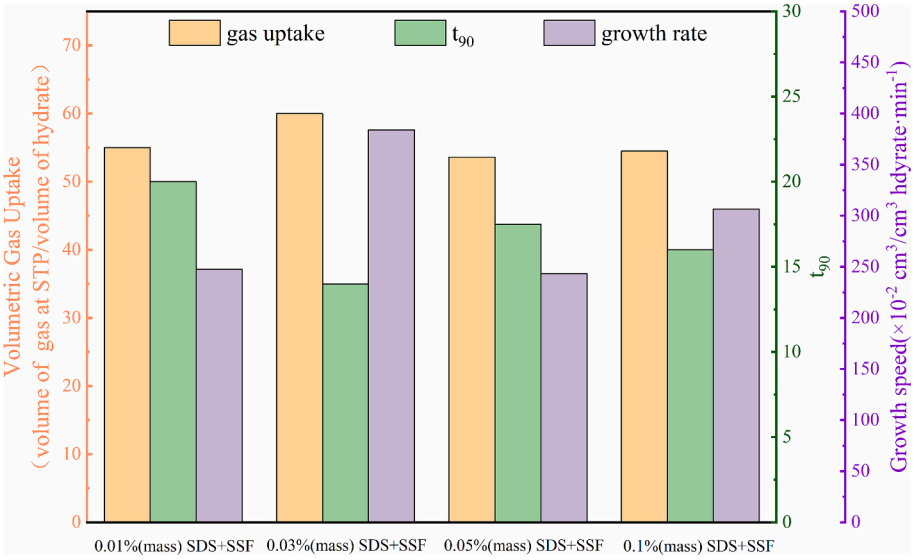

Fig. 5. Comparison of hydrogen storage capacity, t_{90}, and growth rate of hydrogen hydrate formation with SSF in different SDS concentration solution (P = 18.2 MPa, T = 274.15 K).

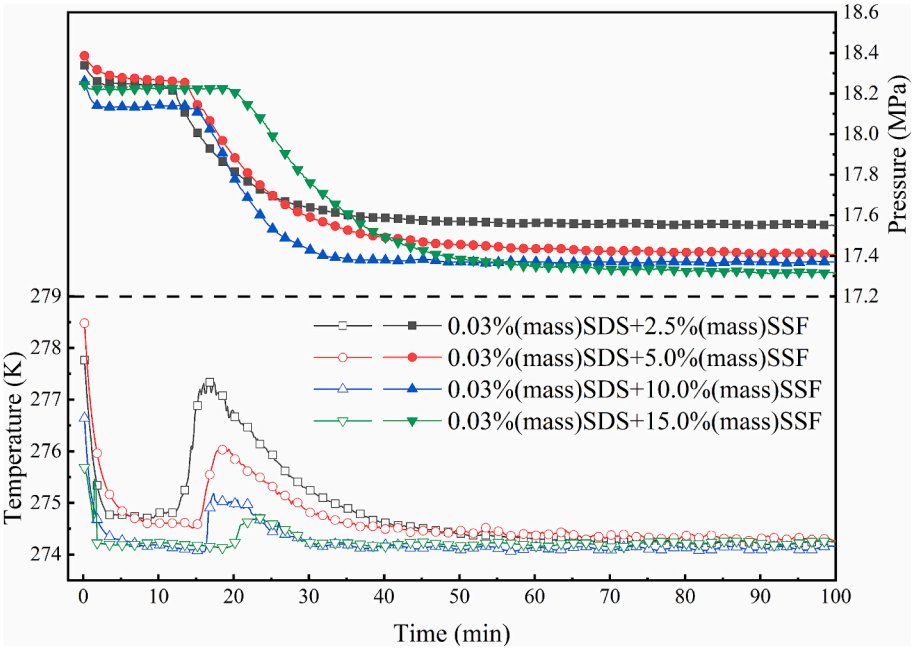

Fig. 6. The variation of temperature and pressure during hydrogen hydrates formation in SDS solution with SSF at 18.2 MPa and 274.15 K.

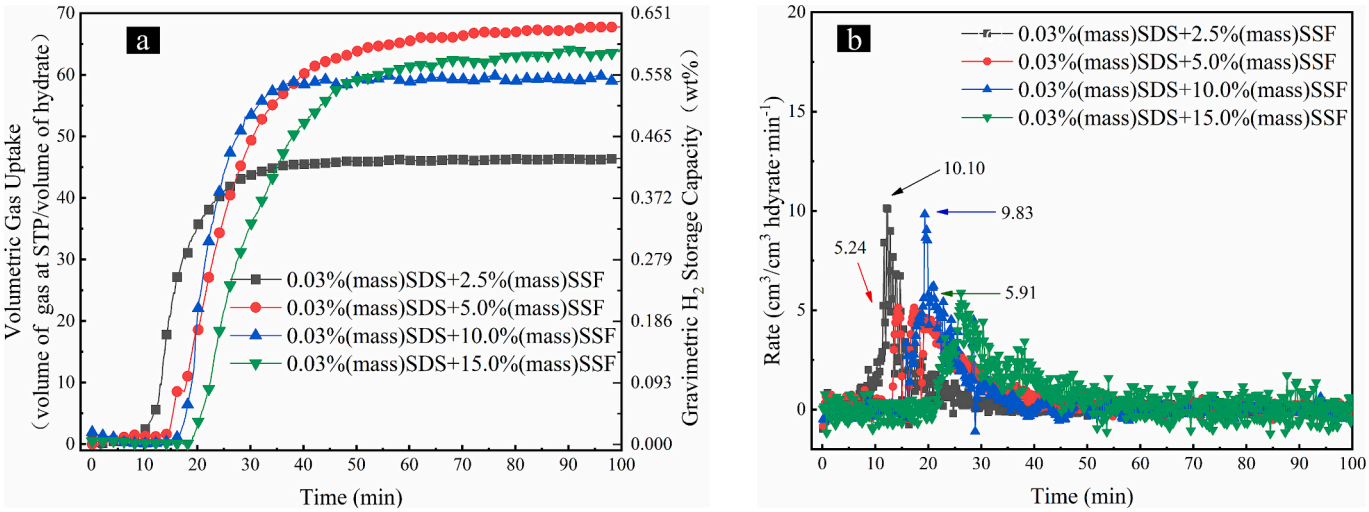

Fig. 7. Effect of SSF amount on hydrogen storage capacity and storage rate (P = 18.2 MPa, T = 274.15 K).

demonstrating a faster and more vigorous hydrate growth process in the long SSF system. Meanwhile, the long SSF system presented obviously faster cooling after the temperature peak, which directly reflected the excellent heat dissipation capability of the continuous linear thermal conduction network constructed by long SSF. In contrast, the short SSF system has a lower temperature peak mainly due to its slower hydrate growth rate and weaker heat release intensity, rather than better heat transfer performance. Therefore, the long SSF system achieved superior comprehensive heat transfer effect despite a higher initial temperature rise, which is responsible for its faster formation kinetics and higher hydrogen storage capacity. The maximum hydrogen storage capacity in the long SSF system reached 69.80 cm^3/cm^3 hydrate—2.51 % higher than that in the short SSF system. Although the gas uptake was only slightly higher, the superior thermal conductivity of long SSF enabled significantly faster growth kinetics: the long SSF system achieved 90 % of the maximum storage capacity in merely 13 min, with an average hydrate growth rate of 483.23 × 10^{-2} cm^3/cm^3 hydrate·min^{-1}—representing a 104.6 % increase compared to the short SSF system. Thus, a continuous heat transfer network facilitates faster hydrate formation kinetics and higher hydrogen storage capacity.

3.4. The promoting effect mechanism of SSF on hydrogen hydrates formation

Substituting the SSF volume fraction (φ≈0.006 %) into Eq. (2) yields the thermal conductivity λ = 0.5701 W·m^{-1}·K^{-1}. It can be seen that ETC remained virtually unchanged. However, the addition of SSF has actually induced a qualitative transformation in the heat transfer behavior. In order to investigate the hydration heat transfer process between hydrate/SSF composites and vessel, a quasi-steady-state one-dimensional radial heat transfer model based on classic hydrate heat transfer modeling was built as described in Fig. 10. The external and internal radiuses of vessel wall were 34 mm (r_0) and 18 mm (r_1), respectively. The following assumptions were presented:

Table 1
Kinetic performance parameters for the experiments conducted in SDS solution with different SSF loading at 274.15 K and an initial pressure of 18.2 MPa.

system	gas storage capacity	Induction time(min)	t_{90} (min)	NRHG ($\times10^{-2}$ cm^3/cm^3 hydrate·min^{-1})
SDS + 2.5 %(mass) SSF	46.25 cm^3/cm^3 hydrate (0.432 wt%)	12	12	346.88
SDS + 5.0 %(mass) SSF	68.09 cm^3/cm^3 hydrate (0.630 wt%)	15	26	235.70
SDS + 10 % (mass) SSF	59.75 cm^3/cm^3 hydrate (0.556 %)	16	14	384.11
SDS + 15 % (mass) SSF	64.09 cm^3/cm^3 hydrate (0.596 wt%)	20	26	262.19

The time from hydrate nucleation to the maximum hydrogen storage of 90 %. Average hydrate growth rate (the average hydrogen storage rate during the process from hydrate nucleation to the maximum gas storage of 90 %.

(1) The SSF was distributed in an interwoven uniform grid pattern, dividing the hydrate formation zone into regular small grids with a side length of a≈1 mm;
(2) Hydrates formed in-situ and fully filled the grids, resulting in a homogeneous two-phase composite system;
(3) Heat transfer was dominated by radial one-dimensional conduction, with axial heat transfer considered negligible;
(4) The hydrate formation process satisfied the quasi-steady state assumption, where the rate of hydrate heat generation equals the rate of heat removal.

The temperature of hydrate/SSF (T_H) was the phase equilibrium temperature under a given pressure, which can be obtained from literature [29]. The external coolant temperature (T_0) was set at 274.15 K and the heat transfer coefficient (α) was 1500 W m^{-2} K^{-1}[32]. During the hydration process, the rate of heat transfer (Q) is presented as a function of three successive thermal resistances:

$$Q = \frac{\Delta T}{R_{total}} = \frac{T_H - T_0}{R_0 + R_w + R_i} \tag{6}$$

where R_{total} is the overall thermal resistance, K W^{-1}. The external coolant resistance (R_0), the vessel wall resistance (R_w) and the internal hydrate resistance (R_i) are expressed by, respectively,

$$R_0 = \frac{1}{\alpha A_0} = \frac{1}{2\pi r_0 H} \tag{7}$$

where α is the convective heat transfer coefficient between the outer wall of the reactor and the cooling medium, W·m^{-2}·K^{-1}; A_0 is the heat transfer area of the outer wall of the reactor, m^2; H is the effective height of the reactor, m.

$$R_w == \frac{1}{2\pi\lambda_w H} In\frac{r_0}{r_1} \tag{8}$$

where λ_w is the thermal conductivity of stainless steel wall, W·m^{-1}·K^{-1}; r_0 and r_1 are the outer radius and inner radius of the reactor, m.

$$R_i == \frac{L_i}{\lambda_w A_i} = \frac{L_i}{\lambda_w \cdot 2\pi r_i H} \tag{9}$$

where L_i is the effective heat conduction distance from hydrate to SSF; taken as approximately 0.005 m under the grid structure.

With the addition of SSF, the hydration heat transfer path was transformed into: Hydrate formation region-SSF grid thermal conductivity network- reactor wall-cooling medium. The effective thermal conduction distance from the hydrate to the heat transfer interface was significantly shortened (the value of L_i was 18 mm to 0.5 mm). Fig. 11 illustrates the effect of SSF on effective thermal conductivity, thermal resistances and heat transfer rate. It could be seen that the volume fraction of SSF was extremely low, leading to a negligible improvement in the macroscopic effective thermal conductivity of the system (from 0.57 W·m^{-1}·K^{-1} to 0.5701 W·m^{-1}·K^{-1}). Without SSF, the overall thermal resistance of hydrogen hydrate was 2.346 K W^{-1} with the value of R_i was 2.278 K W^{-1}, which indicated that the dominant thermal resistance was the internal hydrate resistance R_i. The addition of SSF brings down the thermal resistance R_i to 0.063 K W^{-1}. Given the results of the thermal conductivity and thermal resistance, it could be referred that

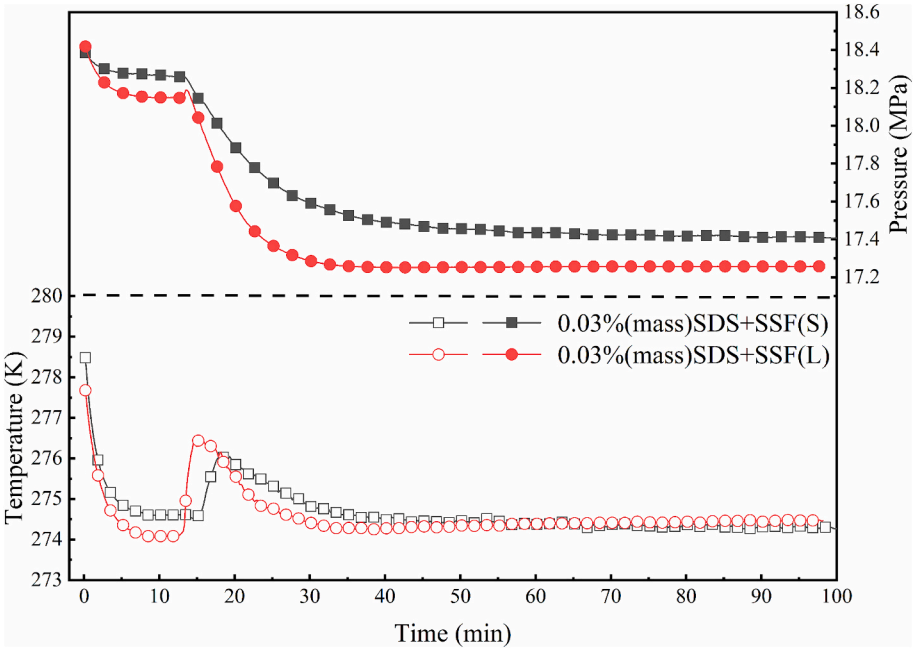

Fig. 8. Changes of temperature and pressure during hydrogen in the presence of different SSF with SDS at 18.2 MPa and 274.15 K.

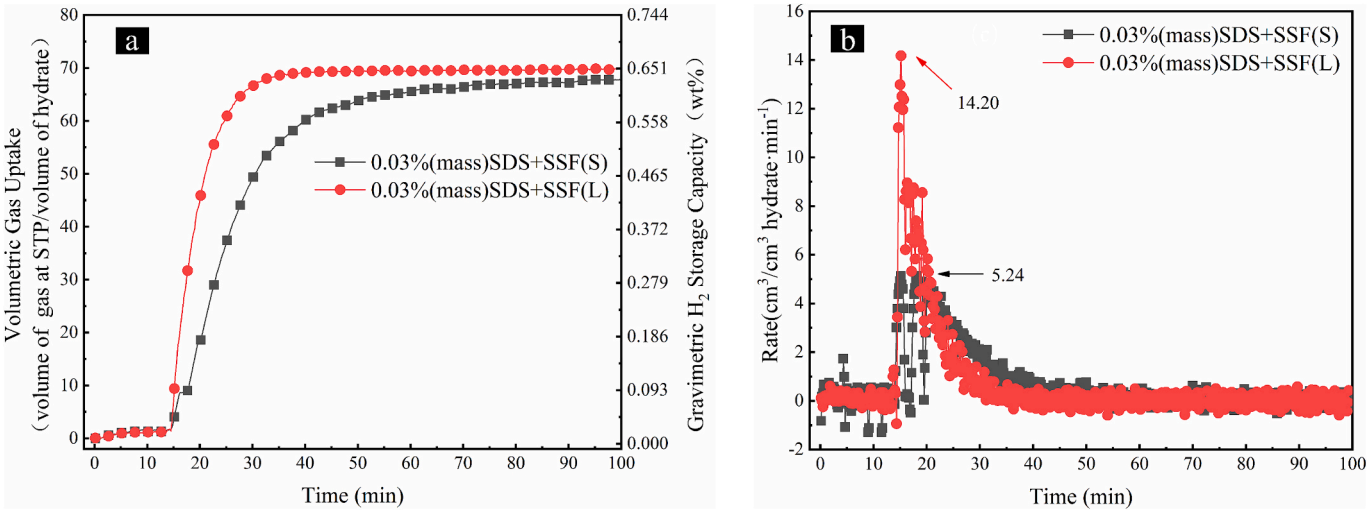

Fig. 9. Effect of different SSF on hydrogen storage capacity and rate (P = 18.2 MPa, T = 274.15 K).

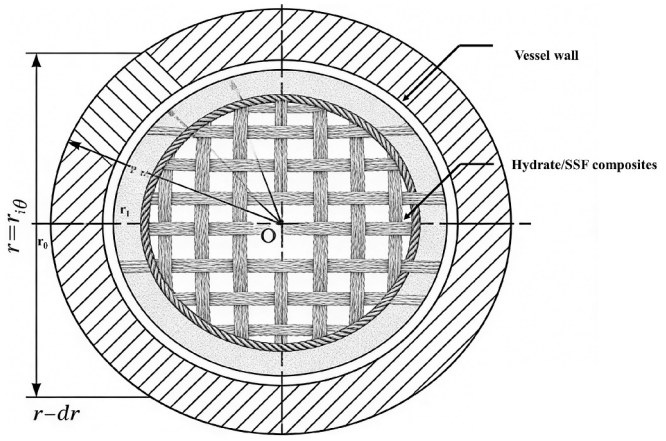

Fig. 10. Schematic heat transfer layers between hydrate/SSF composites and vessel.

the core enhancement stems from a combination of grid segmentation with linear thermal conduction network. The interwoven SSF cuts the hydrate formation zone into numerous small grids, with hydrates only need to transfer heat to the nearest fibers (distance < 1 mm). Horizontal fibers connect directly to the reactor wall, creating a bypass for long-distance radial heat conduction. The dominant thermal resistance was almost effectively eliminated, which the overall thermal resistance R was reduced by 94.4 %. The hydration heat removal rate was significantly improved. Under the same heat transfer temperature difference, the heat removal rate of the system with SSF grids was approximately 18.1 times that of the blank system, which effectively avoids hydration heat accumulation and continuously enhances hydrate growth.

4. Conclusion

The quasi-simultaneous formation (q-SF) approach altered the inherent nucleation mode of hydrogen hydrates. However, the rapid hydrate growth process induced by q-SF exacerbated the hydration heat issue, which in turn inhibited further growth of hydrogen hydrates. To address the heat transfer limitation, highly thermally conductive SSF were incorporated into the system. This study systematically investigated the kinetics of hydrogen hydrate in SDS solutions with SSF, with a specific focus on analyzing the effects of SDS concentration, SSF loading, and SSF structural properties on hydrate-based hydrogen storage kinetics.

1) A synergistic effect was observed between SDS and SSF in promoting hydrate formation, and the synergy was highly dependent on SDS concentrations. The optimal hydrogen storage kinetics were achieved at the SDS concentration of 0.03 % (mass): compared to systems with other SDS concentrations, the hydrogen uptake increased by 9.09 %–11.94 %, and the average hydrate growth rate was significantly enhanced by 25.30 %–57.65 %.
2) The promotional effect on hydrate formation was optimized when the SSF was sufficient to fully cover the gas–liquid interface (5.0 % (mass)). This loading enabled dual enhancement of hydrate nucleation and hydrate growth. Notably, further increasing the SSF loading beyond this optimal value did not yield additional improvements in hydrate formation performance.
3) The system incorporating longer SSF exhibited superior thermal conductivity compared to that with shorter SSF. The maximum hydrogen storage capacity in the long SSF system reached 69.80 cm^3/cm^3 hydrate (0.65 wt%), accompanied by the faster formation kinetics: t_{90} was merely 13 min, and the average hydrate growth rate reached 483.23 × 10^{-2} cm^3/cm^3 hydrate·min^{-1}. While maintaining a comparably high hydrogen storage capacity, this growth rate represented a 67.04 % increase relative to the fastest hydrate-based hydrogen storage kinetics reported in previous studies.
4) The results demonstrated that SSF played a dual role in enhancing hydrate formation: first, it provided abundant nucleation sites for crystallization, shortening the induction time and accelerating the nucleation process; second, it formed an interconnected heat transfer network, which significantly reduced the thermal resistance of hydrate formation zone by 94.4 % to 0.063 K W^{-1}, thereby facilitating sustained hydrate growth by efficiently dissipating hydration heat.

In conclusion, the construction of a continuous heat transfer network (using SSF) facilitates both faster hydrate formation kinetics and higher gas storage. This study provides valuable insights for the development of rapid and efficient hydrate-based hydrogen storage technologies in static systems. The future research can be carried out to verify the enhancement effect of the SSF-SDS system under more engineering-like conditions. And recyclable or magnetically separable thermally conductive fibers could be developed to realize the recycling of additives and reduce industrial costs.

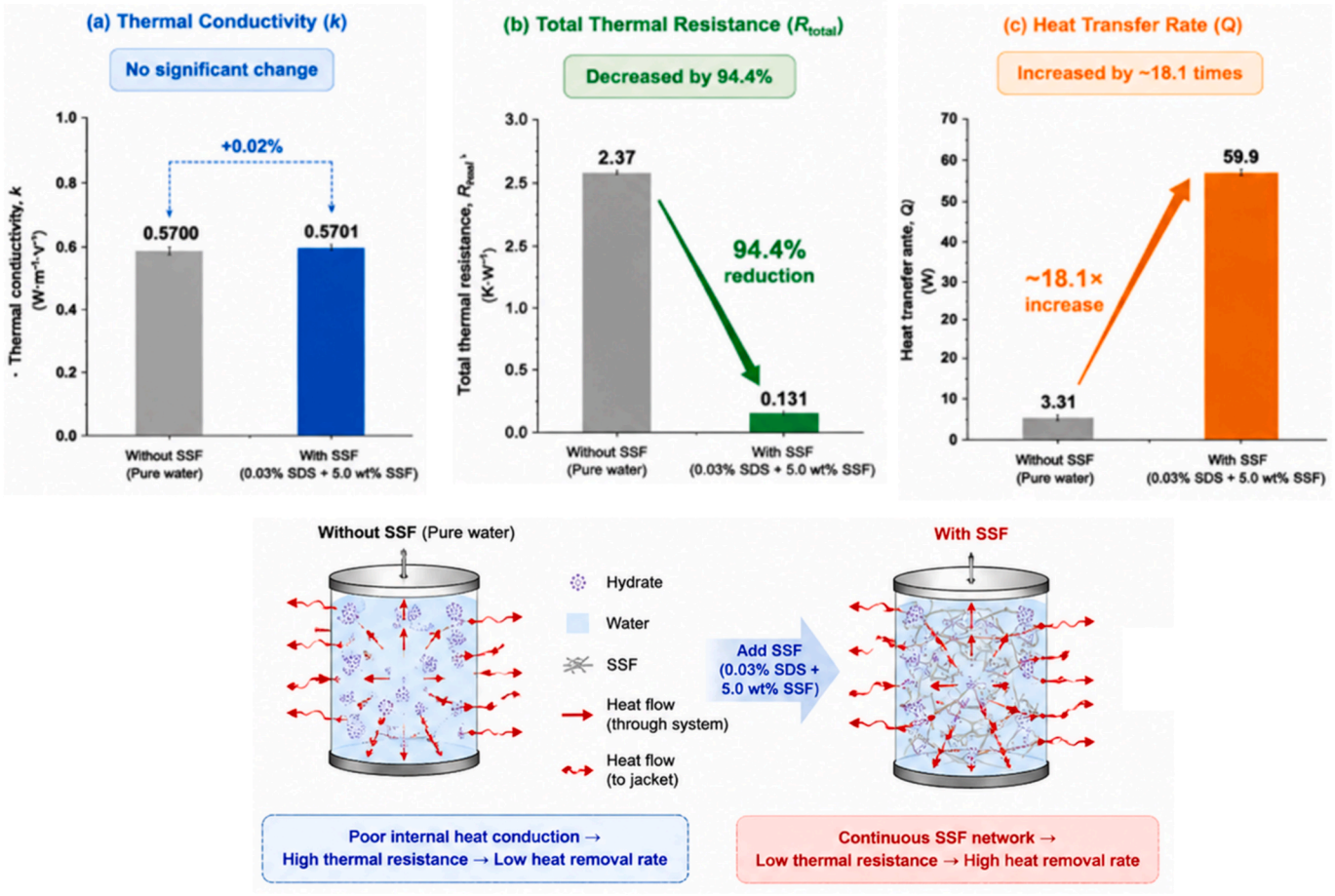

Fig. 11. Influence of stainless steel fibers (SSF) on thermal conductivity, thermal resistance, and heat transfer rate of hydrogen hydrates.

CRediT authorship contribution statement

Siyuan Chen: Writing – original draft, Methodology, Formal analysis. **Yanhong Wang:** Writing – review & editing, Project administration, Conceptualization. **Shuanshi Fan:** Supervision, Funding acquisition. **Xuemei Lang:** Data curation. **Gang Li:** Validation.

Declaration of competing interest

The authors declare that they have no known competing financial interests or personal relationships that could have appeared to influence the work reported in this paper.

Acknowledgements

This work was supported by the National Natural Science Foundation of China (No. 52576205).

Data availability

Data will be made available on request.

References

[1] Khan MN. Hydrogen as future sustainable energy resource: an insight into technological advancements in hydrate-based hydrogen storage. Int J Hydrogen Energy 2025;97:1386–98.
[2] Mao WL. Hydrogen clusters in clathrate hydrate. Science 2002;297:2247–9.
[3] Florusse LJ, Peters CJ, Koh CA, et al. Stable low-pressure hydrogen clusters stored in a binary clathrate hydrate. Science 2004;306:469–71.
[4] Chen SY, Wang YH, Fan SS, et al. Phase equilibrium of hydrogen clathrate hydrates with propylene oxide and 1,2-epoxycyclopentane. J Chem Eng Data 2023;68:1184–90.
[5] Wang YH, Chen SY, Fan SS, et al. Hydrate phase equilibrium of hydrogen with THP, DCM, TBAB+THF and sulfur hexafluoride +TBAB aqueous solution systems. Fluid Phase Equilib 2025;590:114282.
[6] Zhang Y, Bhattacharjee G, Linga P, et al. Hydrogen storage as clathrate hydrates in the presence of 1,3-dioxolane as a dual-function promoter. Chem Eng J 2022;427:131771.
[7] Fan ZM, Wang YH, Fan SS, et al. High-capacity and rapid hydrogen storage in 1,3-dioxolane-H_2 hydrate via pre-wetted bamboo charcoal. Int J Hydrogen Energy 2026;219:154003.
[8] Hondo E, Vishwakarma G, Linga P, et al. Hydrogen storage via clathrate hydrates under mild conditions enabled by mixed cyclic ether synergy. Chem Eng J 2025;524:169469.
[9] Zhang SX, Chen GJ, Guo TM, et al. Hydrate formation of hydrogen + hydrocarbon gas mixtures. J Chem Eng Data 2000;45:908–11.
[10] Mahant B, Kushwaha OS, Kumar R. Thermodynamic phase equilibria study of Hythane (methane + hydrogen) gas hydrates for enhanced energy storage applications. Fluid Phase Equilib 2024;582:114089.
[11] Wang PF, Li KH, Teng Y, et al. Experimental and theoretical study on dissociation thermodynamics and kinetics of hydrogen-propane hydrate. Chem Eng J 2021;426:131279.
[12] Abbondondola JA, Fleischer EB, Janda KC. Comparative study of hydrogen, argon, and xenon uptake into a propane hydrate. AIChE J 2010;56:2734–41.
[13] Wang PF, Long H, Teng Y, et al. Investigation of hydrogen-propane hydrate formation mechanism and optimal pressure range via hydrate-based hydrogen storage. Fuel 2024;361:130791.
[14] Park DH, Lee BR, Lee KH, et al. Gas-hydrate phase equilibrium for mixtures of sulfur hexafluoride and hydrogen. J Chem Eng Data 2012;57:1433–6.
[15] Chen SY, Li XY, Wang YH, et al. Efficient hydrogen storage in hydrate solid solution: structural insights and performance. Int J Hydrogen Energy 2026;204:153331.
[16] Lee W, Ahn YH, Lee JW, et al. Perspectives on facilitating natural gas and hydrogen storage in clathrate hydrates under a static system. Green Chem 2024;26:7552–78.
[17] Li Y, Gambelli AM, Rossi F. Experimental study on the effect of SDS and micron copper particles mixture on carbon dioxide hydrates formation. Energies 2022;15(18):6540.

[18] Chen C, Yuan HY, Wang F, et al. Magnetic nanopromoter enables excellent kinetic promotion and cycling performance in methane hydrate formation. Chem Eng J 2023;452:139318.
[19] Yue PF, Cui XY, Liu ZM, et al. Microporous metal mesh as a tetrabutylammonium bromide carrier promoting natural gas hydrate formation in static systems. Fuel 2027;427:139680.
[20] Zhang CS, Lv QN, Li XS, et al. Promoting effect of through-hole metal foam on hydrogen hydrate formation. Energy Fuel 2026;40:9390–400.
[21] Liu Y, Chen ZR, Chen C, et al. Metal nanoparticle-enhanced gas hydrate growth with sodium dodecyl sulfate: a microscopic simulation study. Cryst Growth Des 2025;25:10281–97.
[22] Wu XG, Shi YQ, Wang L. Kinetic characterization of CH_4 hydrate formation in metal–organic framework nanomaterials and l-Tryptophan complex systems. Energy Fuel 2025;39:10544–53.
[23] Deng ZX, Fan SS, Wang YH, et al. Enhance hydrates formation with stainless steel fiber for high capacity methane storage. Chin J Chem Eng 2022;50:435–43.
[24] Yang L, Liu ZZ, Liu DP, et al. Enhanced natural gas hydrates formation in the suspension with metal particles and fibers. J Mol Liq 2020;301:112410.
[25] Chen SY, Wang YH, Fan SS, et al. An innovative nucleation method for high and rapid hydrogen storage based on clathrate hydrates. J Mater Chem A 2024; 11424–38.
[26] Kashchiev D, Firoozabadi A. Induction time in crystallization of gas hydrates. J Cryst Growth 2003;250:499–515.
[27] Li DL, Peng H, Liang DQ. Thermal conductivity enhancement of clathrate hydrate with nanoparticles. Int J Heat Mass Transf 2017;104:566–73.
[28] Maxwell JC. A treatise on electricity and magnetism. Oxford University Press; 1998.
[29] Huang DZ, Fan SS. Thermal conductivity of methane hydrate formed from sodium dodecyl sulfate solution. J Chem Eng Data 2004;49:1479–82.
[30] Kumar A, Bhattacharjee G, Kumar R, et al. Role of surfactants in promoting gas hydrate formation. Ind Eng Chem Res 2015;54:12217–32.
[31] Wang HF, Wang FX, Yuan W, et al. Experimental investigation on the thermal performance of a heat sink filled with porous metal fiber sintered felt/paraffin composite phase change material. Appl Energy 2016;176:221–32.
[32] Chen C, Yuan H, Wang F, et al. Recyclable and high-efficiency methane hydrate formation promoter based on SDS-coated superparamagnetic nano-Fe_3O_4. Chem Eng J 2022;437:135365.
[33] He Y, Sun MT, Chen C, et al. Surfactant-based promotion to gas hydrate formation for energy storage. J Mater Chem A 2019;7:21634–61.
[34] Gayet P, Dicharry C, Marion G, et al. Experimental determination of methane hydrate dissociation curve up to 55MPa by using a small amount of surfactant as hydrate promoter. Chem Eng Sci 2005;60:5751–8.
[35] Veluswamy HP, Chen JY, Linga P. Surfactant effect on the kinetics of mixed hydrogen/propane hydrate formation for hydrogen storage as clathrates. Chem Eng Sci 2015;126:488–99.
[36] Lim YA, Kumar R, Linga P, et al. Morphology of carbon dioxide–hydrogen–cyclopentane hydrates with or without sodium dodecyl sulfate. Cryst Growth Des 2013;13:2047–59.
[37] Jing X, Fu Z, Jiang R, et al. Sodium dodecyl sulfate induced formation of a messy structure methane hydrate: a molecular dynamics simulation study. Acta Crystallogr B 2026;82:203–8.
[38] Li C, Wu W, Zhang Z, et al. High storage capacity and rapid methane hydrate formation using a novel nonfoaming durfactant. Energy Fuel 2026;40:7308–20.
[39] Kadu H, Sudeeksha LA, Veluswamy HP. Synergistic role of tetrahydrofuran and cyclopentane in hydrogen hydrate formation: a dual-promoter strategy for hydrogen storage. Ind Eng Chem Res 2026;65:6980–93.
[40] Cai X, Salvalaglio M, Striolo A. The quasi-liquid layer thickness controls clathrate hydrates' growth rate. Proc Natl Acad Sci 2026;123:e2521343123.
[41] Wang YF, Qi ZG, Liu J, et al. Mechanistic insight into the "intermediate effect": competitive adsorption and surface coverage model in controlling hydrate formation in a closed-cell foam–SDS system. Chem Eng J 2026;538:176942.
[42] Yang L, Wang J, Liu N, et al. Clathrate hydrate framework construction enhanced by waste bio-shavings for efficient methane storage. ACS Sustain Chem Eng 2022; 10:12127–38.